

Low-order preconditioning of the Stokes equations

Alexey Voronin¹ | Yunhui He² | Scott MacLachlan³ | Luke N. Olson¹ | Raymond Tuminaro⁴

¹Department of Computer Science,
University of Illinois at
Urbana-Champaign, Urbana IL, USA

²Department of Applied Mathematics,
University of Waterloo, Waterloo ON,
Canada

³Department of Mathematics and Statistics,
Memorial University of Newfoundland,
St. John's NL, Canada

⁴Computational Mathematics, Sandia
National Laboratories, Livermore CA, USA

Correspondence

*Alexey Voronin. Department of Computer
Science. University of Illinois at
Urbana-Champaign. Email:
voronin2@illinois.edu

Summary

A well-known strategy for building effective preconditioners for higher-order discretizations of some PDEs, such as Poisson's equation, is to leverage effective preconditioners for their low-order analogs. In this work, we show that high-quality preconditioners can also be derived for the Taylor-Hood discretization of the Stokes equations in much the same manner. In particular, we investigate the use of geometric multigrid based on the \mathbb{Q}_1 iso $\mathbb{Q}_2/\mathbb{Q}_1$ discretization of the Stokes operator as a preconditioner for the $\mathbb{Q}_2/\mathbb{Q}_1$ discretization of the Stokes system. We utilize local Fourier analysis to optimize the damping parameters for Vanka and Braess-Sarazin relaxation schemes and to achieve robust convergence. These results are then verified and compared against the measured multigrid performance. While geometric multigrid can be applied directly to the $\mathbb{Q}_2/\mathbb{Q}_1$ system, our ultimate motivation is to apply algebraic multigrid within solvers for $\mathbb{Q}_2/\mathbb{Q}_1$ systems via the \mathbb{Q}_1 iso $\mathbb{Q}_2/\mathbb{Q}_1$ discretization, which will be considered in a companion paper.

KEYWORDS:

Monolithic Multigrid, Stokes Equations, Braess-Sarazin, Additive Vanka, Local Fourier Analysis

1 | INTRODUCTION

This paper focuses on developing efficient algorithms for the numerical approximation of solutions to the Stokes equations, which are used to simulate incompressible viscous flow and whose discretization results in saddle-point linear systems¹. Linear systems of saddle-point type appear in a variety of scientific and engineering applications². The block structure and indefiniteness of these systems often make it particularly challenging to construct efficient numerical schemes. The coupled physical fields, pressure and velocity, are often discretized using staggered grids or methods where degrees of freedom are not located at the same spatial point, further complicating the development of solvers such as monolithic multigrid for these systems.

Monolithic multigrid methods, that apply multigrid to the entire system in a coupled (or all-at-once) manner, have long demonstrated robust convergence for Stokes problems^{3–17}. Most of these approaches are geometric multigrid (GMG) methods, where the multigrid hierarchy is composed of a sequence of coarser discretizations on nested meshes, connected by canonical interpolation operators for each field. There are many fewer approaches to monolithic algebraic multigrid (AMG) for Stokes and similar systems^{10, 11, 13, 16}, as algebraic coarsening of these matrices is complicated by the presence of higher-order finite-element bases, which are present in a majority of stable Stokes discretizations. This is in part due to two main obstacles. First, the stiffness matrices constructed with higher-order basis functions are no longer M-matrices, for which AMG methods were originally intended^{18, 19}. Secondly, the coarsening of one field cannot be done independently of the other, due to *inf-sup* stability concerns^{10, 11, 13, 16}. In order to address the first obstacle, we propose to coarsen with respect to the element order (p) and, then, to employ geometric multigrid on the low-order system by coarsening spatially in h . This does require that a low-order system be constructed, however, it is facilitated by the standard building blocks needed to build the high-order discretization. While the

approach presented here is one of geometric multigrid, we propose this primarily as a building block that can be leveraged in future AMG work that will aim to address the second obstacle.

Low-order preconditioning is a common approach when developing preconditioners for higher-order discretizations. These methods have been successfully used for preconditioning discretized Laplace operators in both geometric and algebraic multigrid contexts^{19–24}. In the case of the Stokes problem, non-nested low-order geometric multigrid methods have been shown to be effective preconditioners for higher-order discretizations²⁵. In this paper, we construct and use a stable lower-order $\mathbb{Q}_1\text{iso}\mathbb{Q}_2/\mathbb{Q}_1$ discretization within a monolithic multigrid preconditioner for the $\mathbb{Q}_2/\mathbb{Q}_1$ discretized Stokes system. While “double discretization” or “defect correction” schemes^{26, 27} and multigrid methods based on low-order discretizations^{10, 28, 29} have been considered before independently of each other, to our knowledge, these schemes have not yet been considered for the stable Taylor-Hood finite-element discretization. The goal of our work is to gauge the effectiveness of this type of preconditioning for this discretization.

A major complication in defect-correction algorithms is the plethora of algorithmic parameters that can arise, including relaxation parameters for both higher-order and lower-order discretizations, and additional parameters related to cycling strategies between the discretizations. Here, we consider both the choice of and sensitivity to these parameters in the context of geometric multigrid, which we use to approximate the inverse of the $\mathbb{Q}_1\text{iso}\mathbb{Q}_2/\mathbb{Q}_1$ system within a standard defect-correction scheme. Using geometric multigrid offers an advantage in that parameter choices can be determined using local Fourier analysis^{30, 31}. Local Fourier analysis has been studied and applied to many interesting problems, including monolithic multigrid methods for the Stokes equations. Indeed, early work in this direction focused on the use of both distributed⁷ and Vanka³² relaxation for the staggered marker-and-cell (MAC) finite-difference discretization scheme for the Stokes equations. More recent Fourier analysis has included that of multiplicative³³ and additive¹⁷ Vanka relaxation for the $\mathbb{Q}_2/\mathbb{Q}_1$ discretization, as well as for Braess-Sarazin relaxation³⁴. Here, we make use of these tools to optimize multigrid parameters in stationary iterations for the proposed defect-correction scheme.

The remainder of the paper is structured in the following manner. In Section 2, we briefly introduce the $\mathbb{Q}_2/\mathbb{Q}_1$ and $\mathbb{Q}_1\text{iso}\mathbb{Q}_2/\mathbb{Q}_1$ discretizations for the Stokes equations. Section 3 describes the monolithic multigrid framework with Braess-Sarazin and additive Vanka relaxation for the Stokes equations, while Section 4 introduces local Fourier analysis (LFA) as a tool to identify optimal GMG parameters. Section 5 exhibits the main contributions of this paper: optimized LFA two-grid convergence factors and the measured multigrid convergence for the Stokes problem. Section 6 presents the conclusions. The main contribution of this work is that of demonstrating that the principle of low-order preconditioning is also applicable to a mixed finite-element discretization such as the $\mathbb{Q}_2/\mathbb{Q}_1$ discretization of Stokes. In our view, this opens a new line of research into the development of truly algebraic multigrid methods for such discretizations, by providing a route to effectively precondition higher-order discretizations without directly applying AMG to them. A central question in that direction that we aim to address in future work is how to algebraically create a hierarchy of stable coarse-grid operators that allow effective multigrid cycling on problems such as the $\mathbb{Q}_1\text{iso}\mathbb{Q}_2/\mathbb{Q}_1$ discretization.

2 | DISCRETIZATION AND SOLUTIONS OF STOKES EQUATIONS

In this paper, we consider the two-dimensional Stokes equations, given by

$$-\nabla^2 \mathbf{u} + \nabla p = \mathbf{f} \quad (1a)$$

$$-\nabla \cdot \mathbf{u} = 0 \quad (1b)$$

where \mathbf{u} is the velocity of the fluid, p is the pressure, and \mathbf{f} is a forcing term. We assume homogenous Dirichlet conditions on \mathbf{u} over the boundary of a domain Ω for simplicity. In addition, we consider a uniform grid of size h over Ω and finite dimensional spaces of the form $\mathcal{X}^h \subset \mathbf{H}_0^1(\Omega)$ and $\mathcal{M}^h \subset L_2(\Omega)$, where \mathcal{X}^h satisfies the appropriate homogeneous Dirichlet boundary conditions. The resulting discrete weak formulation of (1) is to find $\mathbf{u} \in \mathcal{X}^h$ and $p \in \mathcal{M}^h$ such that

$$a(\mathbf{u}, \mathbf{v}) + b(p, \mathbf{v}) = F(\mathbf{v}) \quad (2a)$$

$$b(q, \mathbf{u}) = 0, \quad (2b)$$

for all $q \in \mathcal{M}^h$ and $\mathbf{v} \in \mathcal{X}^h$. Here, $a(\cdot, \cdot)$ and $b(\cdot, \cdot)$ are bilinear forms and $F(\cdot)$ is a linear form given by

$$a(\mathbf{u}, \mathbf{v}) = \int_{\Omega} \nabla \mathbf{u} : \nabla \mathbf{v}, \quad b(p, \mathbf{v}) = - \int_{\Omega} p \nabla \cdot \mathbf{v}, \quad F(\mathbf{v}) = \int_{\Omega} \mathbf{f} \cdot \mathbf{v}.$$

An *inf-sup* condition on the finite-dimensional spaces \mathcal{X}^h and \mathcal{M}^h is sufficient to guarantee the uniqueness of the solution up to a constant pressure¹.

Our focus is on two types of stable mixed finite-element discretizations for \mathcal{X}^h and \mathcal{M}^h . The first is the $\mathbb{Q}_2/\mathbb{Q}_1$ discretization (also known as the *Taylor-Hood* discretization), which uses a bilinear representation of the pressure and a biquadratic representation for the velocity components. The second is the $\mathbb{Q}_1\text{iso}\mathbb{Q}_2/\mathbb{Q}_1$ discretization, which replaces the \mathbb{Q}_2 space for velocities with an \mathbb{Q}_1 approximation on a once-refined mesh. This is obtained by overlaying the higher-order nodes with a lower-order mesh — see Figure 1. The $\mathbb{Q}_1\text{iso}\mathbb{Q}_2/\mathbb{Q}_1$ discretization is not well-known due to its relatively low accuracy and computational efficiency. Yet, the pairing is known to be *inf-sup* stable³⁵, and we argue that it can be highly effective when used within a preconditioner for the $\mathbb{Q}_2/\mathbb{Q}_1$ discretization, by leveraging efficient first-order multigrid solvers.

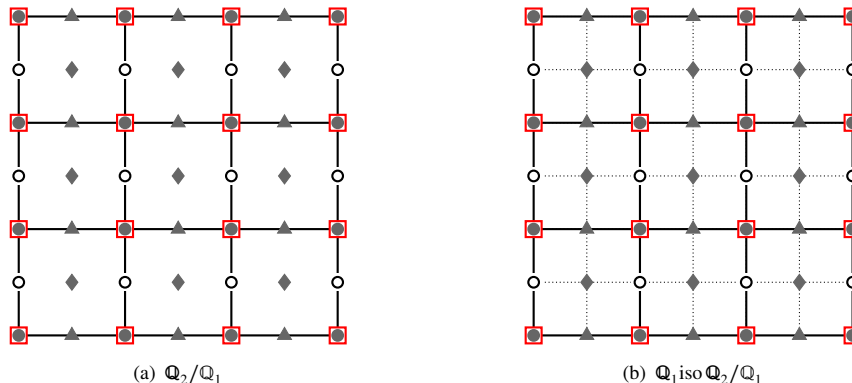


FIGURE 1 Meshes and degrees of freedom for the $\mathbb{Q}_2/\mathbb{Q}_1$ and $\mathbb{Q}_1\text{iso}\mathbb{Q}_2/\mathbb{Q}_1$ discretizations. Dark markers [●, ○, ▲, ◆] correspond to the velocity locations (two components of velocity per marker), and red squares □ correspond to the pressure locations.

The challenge presented by the discretization in (2) is the solution of the resulting saddle-point system of the form

$$K \begin{bmatrix} \mathbf{u} \\ p \end{bmatrix} = \begin{bmatrix} A & B^T \\ B & 0 \end{bmatrix} \begin{bmatrix} \mathbf{u} \\ p \end{bmatrix} = \begin{bmatrix} \mathbf{f} \\ 0 \end{bmatrix} = \mathbf{b}, \quad (3)$$

where matrix A corresponds to the discrete vector-Laplacian, and B represents the negative of the discrete divergence operator. Here, we overload the notation and use \mathbf{u} and p to denote the discrete velocities and pressure for the remainder of the paper. We note that, for the boundary conditions described above, the matrix K is singular, with a one-dimensional nullspace associated with constant shifts in the pressure. While many “fixes” to this nullspace are used in practice (e.g., fixing the value of the pressure at a point, or explicitly adding a constraint that the integral of the pressure is zero), we will leave the system in its singular form and implicitly treat the nullspace in our multigrid method.

3 | MONOLITHIC MULTIGRID

We study a monolithic geometric multigrid approach with standard coarsening — i.e., doubling h on each level of the hierarchy. In the following, we assess the error reduction in multigrid when using a coupled relaxation method followed by a coarse-grid correction. Interpolation and restriction are constructed using the finite element basis. In the following, we use ℓ to denote the level of the multigrid hierarchy with $\ell = 0$ denoting the finest-level problem. The subscript may be dropped when context is clear.

For a linear system $K_\ell u_\ell = b_\ell$ on level ℓ of the multigrid hierarchy, we express the relaxation scheme as a fixed-point iteration

$$u_\ell^{j+1} = (I - \omega_\ell M_\ell^{-1} K_\ell) u_\ell^j + \omega_\ell M_\ell^{-1} b_\ell,$$

where M_ℓ is an inexpensive approximation to K_ℓ so that the action of its inverse is easy to apply. Here, $(I - \omega_\ell M_\ell^{-1} K_\ell)$ is the associated error-propagation operator for relaxation on K_ℓ , where ω_ℓ is a damping parameter. Using restriction R_ℓ and interpolation P_ℓ , the coarse-grid correction operator projects the error onto grid $\ell + 1$, where a correction is computed. Combining pre- and post-relaxation together with coarse grid correction we arrive at the two-grid error-propagation operator

$$G_\ell = (I - \omega_\ell M_\ell^{-1} K_\ell)(I - P_\ell K_{\ell+1}^{-1} R_\ell K_\ell)(I - \omega_\ell M_\ell^{-1} K_\ell) \quad (4)$$

when one sweep of pre- and one sweep of post-relaxation is applied within the multigrid cycle. The coarse-grid operators for the $\mathbb{Q}_1 \text{ iso } \mathbb{Q}_2 / \mathbb{Q}_1$ system are computed via the Galerkin product $K_{\ell+1} = R_\ell K_\ell P_\ell$, which is equivalent to rediscrretization on the coarse grids. The correction on the coarsest grid is computed using a pseudoinverse, to account for the pressure nullspace.

3.1 | Low-order Preconditioner

Lower-order preconditioning has been successfully used for a variety of problems, ranging from elliptic PDEs to saddle-point systems^{19, 22, 23, 36}. For example, taking A_0 to be the matrix from a high-order spectral discretization of the Laplace operator and A_1 to be the matrix from a second-order finite-difference discretization on an auxiliary mesh constructed from the nodal points of the high-order mesh, then the condition number of $A_1^{-1} A_0$ is bounded asymptotically by $\pi^2/4$ ^{20, 37}, establishing A_1 as an effective preconditioner for A_0 .

Here, we consider a multigrid defect-correction method that incorporates this notion of high- and low-order operators. This is constructed by taking K_0 and K_1 to be the higher-order and lower-order Stokes operators assembled using the $\mathbb{Q}_2 / \mathbb{Q}_1$ and $\mathbb{Q}_1 \text{ iso } \mathbb{Q}_2 / \mathbb{Q}_1$ finite element spaces, respectively. Note that the $\mathbb{Q}_1 \text{ iso } \mathbb{Q}_2 / \mathbb{Q}_1$ discretization is not a Galerkin coarsening of the $\mathbb{Q}_2 / \mathbb{Q}_1$ discretization, as the finite-element spaces are not nested. That is, $K_1 \neq R_0 K_0 P_0$ within this multigrid hierarchy. Since the unknowns for levels 0 and 1 are, however, co-located, we transfer residuals and corrections between the low- and high-order discretizations using identity operators, effectively taking $P_0 = I$ and $R_0 = I$. On level 1, we then use γ iterations of monolithic GMG based on the K_1 system, which is denoted as G_1 . The level-1 multigrid cycle is represented by $\tau(I - G_1^\gamma)K_1^{-1}$, which leads to a generalization of (4) for $\ell = 0$

$$E = (I - \omega_0 M_0^{-1} K_0)^{\nu_2} (I - \tau(I - G_1^\gamma)K_1^{-1} K_0) (I - \omega_0 M_0^{-1} K_0)^{\nu_1}, \quad (5)$$

where M_0 is a relaxation operator based on the K_0 system, ω_0 is the relaxation parameter, γ is the number of level-1 h -multigrid cycles used to approximately solve the K_1 problem, τ is a damping parameter for the coarse correction, and the exponents ν_1 and ν_2 are the number of pre- and post- relaxation sweeps.

The multigrid scheme in (5) is depicted in Figure 2. If $\gamma = 0$, then the method relaxes *only* on the $\mathbb{Q}_2 / \mathbb{Q}_1$ problem and the $\mathbb{Q}_1 \text{ iso } \mathbb{Q}_2 / \mathbb{Q}_1$ discretization is unused. At the same time, if $G_1^\gamma \equiv 0$ in (5), then the $\mathbb{Q}_1 \text{ iso } \mathbb{Q}_2 / \mathbb{Q}_1$ problem is solved *exactly*. The left image in Figure 2 illustrates the case where the overall multigrid cycle employs two-level (blue) and multilevel (green) h -multigrid schemes for the $\mathbb{Q}_1 \text{ iso } \mathbb{Q}_2 / \mathbb{Q}_1$ part of the cycle with $\gamma = 1$. The right image shows $\gamma = 2$ for a two-level scheme. In the following tests, we study multigrid convergence over a range of parameters, possibly omitting relaxation on different levels. For the remainder of the paper, the terms two-level, and multilevel always refer to the number of levels associated with only the GMG (or h -multigrid) part of the overall cycle defined by (5).

3.2 | Relaxation

The relaxation method M_ℓ^{-1} applied to the saddle-point system K_ℓ is either chosen as an additive Vanka^{17, 38} or Braess-Sarazin⁸ coupled relaxation scheme. In this section, we drop the operator subscript ℓ , since the relaxation operator construction is the same on all levels of the multigrid hierarchy.

Letting n_p be the number of pressure degrees of freedom (DoFs), Vanka relaxation partitions the $n \times n$ system K into n_p overlapping saddle-point problems, consisting of 2×2 patches of elements around each nodal pressure DoF. An important feature of the construction of Vanka relaxation (in contrast to so-called ‘‘star’’ relaxation³⁹) is that each patch consists of all velocity degrees of freedom that are on the closure of the elements adjacent to the nodal pressure DoF, and not just those in the interior of mesh entities (elements and faces) adjacent to the node. Each patch contains a single pressure DoF, however. Figure 3 shows the construction of a Vanka patch for both the $\mathbb{Q}_2 / \mathbb{Q}_1$ and $\mathbb{Q}_1 \text{ iso } \mathbb{Q}_2 / \mathbb{Q}_1$ discretizations; it is important to note that the construction of the Vanka patches in the $\mathbb{Q}_1 \text{ iso } \mathbb{Q}_2 / \mathbb{Q}_1$ discretization is based on the (coarse) pressure elements and not the (fine) velocity elements. For each patch, indexed by pressure DoF i , we form a (binary) restriction operator, V_i , which selects those entries in a

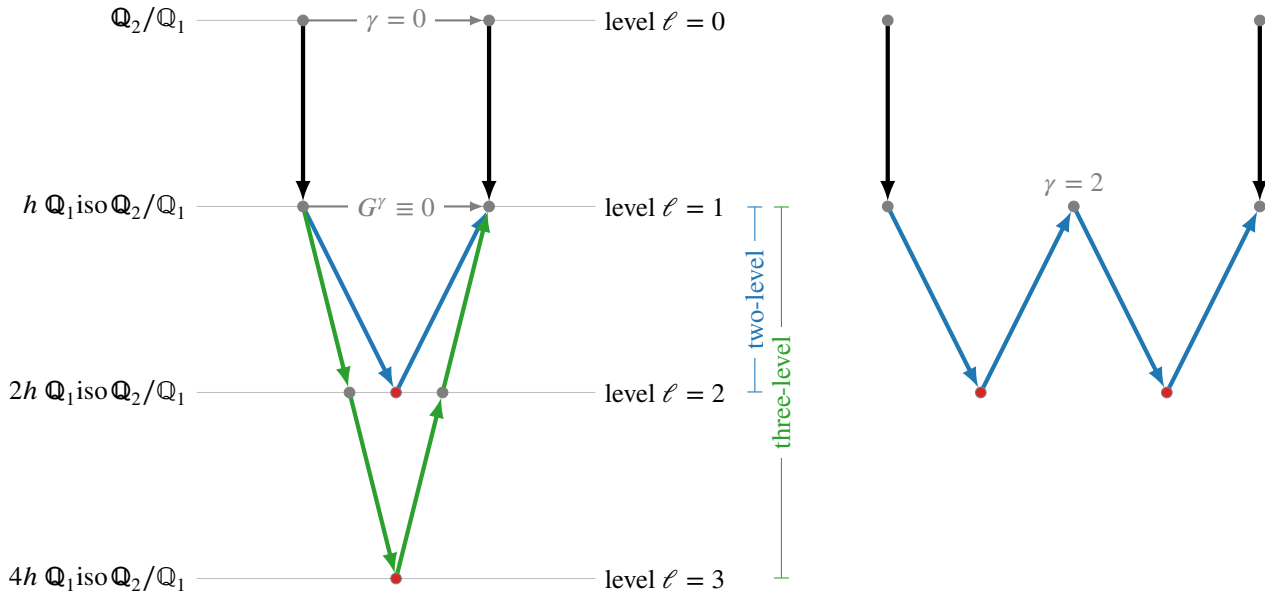


FIGURE 2 Multilevel scheme for the $\mathbb{Q}_2/\mathbb{Q}_1$ operator. Coarse levels are refinements in h on the $\mathbb{Q}_1 \text{ iso } \mathbb{Q}_2/\mathbb{Q}_1$ discretization, resulting in either a two-level scheme (blue) or a multilevel scheme (green). On the left, a single V-cycle is executed on the $\mathbb{Q}_1 \text{ iso } \mathbb{Q}_2/\mathbb{Q}_1$ problem (with $\gamma = 1$); on the right, two V-cycles are executed (with $\gamma = 2$). The exact, coarsest level solves are marked in red.

global vector that appear on patch i . The system matrix is then projected onto the patch DoFs by a triple matrix product, $V_i K V_i^T$. A single iteration of Vanka is then given by

$$M_V^{-1} = \sum_{i=1}^{n_p} V_i^T W_i (V_i K V_i^T)^{-1} V_i,$$

where the diagonal weighting matrix W_i is defined such that each diagonal entry is equal to the reciprocal of the number of patches that contain the associated degree of freedom.

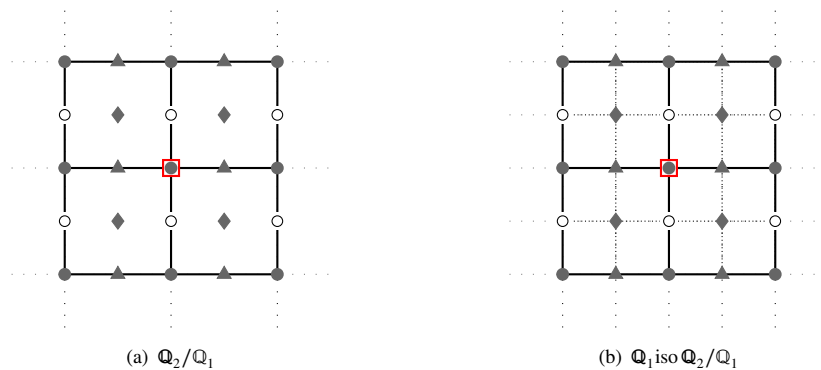


FIGURE 3 At left, construction of a typical Vanka patch for the $\mathbb{Q}_2/\mathbb{Q}_1$ discretization. At right, construction of a typical Vanka patch for the $\mathbb{Q}_1 \text{ iso } \mathbb{Q}_2/\mathbb{Q}_1$ discretization. Note that the patch in (b) includes one pressure DoF and all the velocity DoFs that geometrically lie within (or on the boundary) of the sub-domain associated with the elements that include that pressure DoF.

In contrast to Vanka relaxation, Braess-Sarazin relaxation retains the block structure of the Stokes system to produce a suitable relaxation method. A single application of Braess-Sarazin relaxation is formulated as the (approximate) solution to the following

system

$$M_{BS}\delta x = \begin{bmatrix} \alpha \tilde{A} & B^T \\ B & 0 \end{bmatrix} \begin{bmatrix} \delta \mathbf{u} \\ \delta p \end{bmatrix} = \begin{bmatrix} r_u \\ r_p \end{bmatrix}, \quad (6)$$

where $\alpha > 0$ is a relaxation parameter, \tilde{A} is some approximation to A , r_u and r_p are the components of the current residual, and $\delta \mathbf{u}$ and δp are the components of the correction. The system in (6) is solved in two sequential steps

$$(B\tilde{A}^{-1}B^T)\delta p = B\tilde{A}^{-1}r_u - \alpha r_p, \quad (7a)$$

$$\delta \mathbf{u} = \frac{1}{\alpha} \tilde{A}^{-1}(r_u - B^T \delta p). \quad (7b)$$

Different Braess-Sarazin variations are devised using different choices for \tilde{A} and whether or not (7a) is solved *exactly*. A common approach is to take \tilde{A} to be the diagonal matrix defined by $\tilde{A}_{ii} = A_{ii}$ for all i . This allows $B\tilde{A}^{-1}B^T$ to be directly computed, as well as matrix-vector products with \tilde{A}^{-1} . Note that the exact solution of (7a) is impractical and, so, we consider the inexact Braess-Sarazin relaxation (IBSR), where (7a) is approximately solved via a single weighted Jacobi iteration, with a weighting factor β .

Both Vanka and IBSR relaxation include several parameters that must be chosen. While parameter choices are known in some cases^{17, 34}, our defect-correction framework is somewhat unique and so we employ LFA to inform our parameter choices for the relaxation methods and for the MG cycle defined by Equations (4) and (5).

4 | LOCAL FOURIER ANALYSIS

LFA is a well-known and valuable tool in predicting and analyzing algorithmic performance for the solution of discretized PDEs^{30, 31}. In particular, LFA is often used to guide parameter choices for multigrid components, including those within relaxation schemes and grid-transfer operators. Here, we apply LFA to the monolithic multigrid methods in Section 3 and aim to optimize the spectral radius of the two-grid error propagation operator (4) over the possible choices of parameters.

4.1 | Definition and notations

For completeness, we give a brief introduction to LFA^{30, 31}. First, consider a two-dimensional infinite uniform grid

$$\mathcal{G} = \{ \mathbf{x} := (x_1, x_2) = (k_1, k_2)h, \quad (k_1, k_2) \in \mathbb{Z}^2 \},$$

with uniform grid size h . Let A be a scalar Toeplitz operator defined by entries in a “stencil”, $s_{\kappa} \in \mathbb{R}$, where $\kappa \in V \subset \mathbb{Z}^2$ is a finite index set over which the stencil is nonzero, that acts on a vector $w(\mathbf{x}) \in l^2(\mathcal{G})$ as follows:

$$Aw(\mathbf{x}) = \sum_{\kappa \in V} s_{\kappa} w(\mathbf{x} + \kappa h).$$

Such operators can be formally diagonalized by the Fourier modes $\psi(\boldsymbol{\theta}, \mathbf{x}) = e^{i\boldsymbol{\theta} \cdot \mathbf{x}/h} = e^{i\theta_1 x_1/h} e^{i\theta_2 x_2/h}$, where $\boldsymbol{\theta} = (\theta_1, \theta_2)$ and $i^2 = -1$. Thus, we use $\psi(\boldsymbol{\theta}, \mathbf{x})$ as a Fourier basis with $\boldsymbol{\theta} \in \left[-\frac{\pi}{2}, \frac{3\pi}{2}\right)^2$. Considering standard coarsening by a factor of 2 in each direction, the relevant spaces of low and high frequencies are given by

$$\boldsymbol{\theta} \in T^{\text{low}} = \left[-\frac{\pi}{2}, \frac{\pi}{2}\right)^2, \quad \boldsymbol{\theta} \in T^{\text{high}} = \left[-\frac{\pi}{2}, \frac{3\pi}{2}\right)^2 \setminus \left[-\frac{\pi}{2}, \frac{\pi}{2}\right)^2.$$

LFA provides two possible predictions of multigrid performance through the so-called “smoothing” and “two-grid convergence” factors, which often offer sharp predictions of actual multigrid performance. Unfortunately, the simpler LFA smoothing factor can provide poor predictions when used on complicated or higher-order operators⁴⁰. Thus, we instead focus here on the two-grid LFA convergence factor, which includes the full details of the coarse-grid correction process. To do this, we define the following harmonic modes

$$\boldsymbol{\theta}^{\xi} = (\theta_1^{\xi_1}, \theta_2^{\xi_2}) = \boldsymbol{\theta} + \pi \cdot \boldsymbol{\xi}, \quad \boldsymbol{\theta} := \boldsymbol{\theta}^{00} \in T^{\text{low}},$$

where $\boldsymbol{\xi} = (\xi_1, \xi_2) \in \{(0, 0), (1, 0), (0, 1), (1, 1)\}$.

Definition 1. For a given Toeplitz operator, A , $\tilde{A}(\boldsymbol{\theta}) = \sum_{\kappa \in V} s_{\kappa} e^{i\boldsymbol{\theta} \cdot \kappa}$ is the symbol of A .

Note that for all Fourier modes, $\psi(\boldsymbol{\theta}, \mathbf{x})$, we have

$$A\psi(\boldsymbol{\theta}, \mathbf{x}) = \tilde{A}(\boldsymbol{\theta})\psi(\boldsymbol{\theta}, \mathbf{x}).$$

If the multigrid relaxation scheme, M , is also represented by a Toeplitz operator (or its inverse), then the symbol for the error-propagation operator $\tilde{S}(\boldsymbol{\theta}) = I - \tilde{M}^{-1}(\boldsymbol{\theta})\tilde{A}(\boldsymbol{\theta})$ provides information on how the relaxation scheme damps errors at each Fourier frequency. The LFA smoothing factor arises from computing the maximum (absolute) value of $\tilde{S}(\boldsymbol{\theta})$ over the high-frequency set, T^{high} .

To get a better picture of multigrid convergence, we study how the relaxation scheme represented by $\tilde{S}(\boldsymbol{\theta})$ interacts with the coarse-grid correction. Here, we must account for the coupling of fine-grid errors in the coarse-grid correction process. For each low-frequency mode, $\boldsymbol{\theta} \in T^{\text{low}}$, we define a four-dimensional harmonic space,

$$F(\boldsymbol{\theta}) = \text{span}\left\{\psi(\boldsymbol{\theta}^\xi, \cdot) : \xi \in \{(0, 0), (1, 0), (0, 1), (1, 1)\}\right\},$$

which is invariant for standard full-coarsening two-grid algorithms under certain assumptions on their grid-transfer operators. The *symbol* of the two-grid algorithm is defined analogously to Definition 1, accounting for how interpolation and restriction map between grids. For the given interpolation and restriction operators, P and R , we can define their symbols by how they map harmonic modes between grids. For interpolation, a single coarse-grid mode with frequency $2\boldsymbol{\theta}$ is mapped onto $F(\boldsymbol{\theta})$, resulting in a 4×1 symbol for P , denoted \tilde{P}_{2g} , with entries corresponding to each harmonic frequency. The restriction is similarly mapped into a 1×4 symbol, \tilde{R}_{2g} , representing how each fine-grid harmonic frequency is mapped onto the coarse-grid mode with frequency $2\boldsymbol{\theta}$. As a result, the symbol of the two-grid error propagation operator is a 4×4 matrix given by

$$\tilde{E}_{2g}(\boldsymbol{\theta}) = \tilde{S}_{2g}^{v_2}(\boldsymbol{\theta}) \left(I - \tilde{P}_{2g}(\boldsymbol{\theta})(\tilde{A}_C(2\boldsymbol{\theta}))^{-1} \tilde{R}_{2g}(\boldsymbol{\theta})\tilde{A}_{2g}(\boldsymbol{\theta}) \right) \tilde{S}_{2g}^{v_1}(\boldsymbol{\theta}), \quad (8)$$

where

$$\begin{aligned} \tilde{A}_{2g}(\boldsymbol{\theta}) &= \text{diag}\left\{\tilde{A}(\boldsymbol{\theta}^{00}), \tilde{A}(\boldsymbol{\theta}^{10}), \tilde{A}(\boldsymbol{\theta}^{01}), \tilde{A}(\boldsymbol{\theta}^{11})\right\}, \\ \tilde{R}_{2g}(\boldsymbol{\theta}) &= \left[\tilde{R}(\boldsymbol{\theta}^{00}), \tilde{R}(\boldsymbol{\theta}^{10}), \tilde{R}(\boldsymbol{\theta}^{01}), \tilde{R}(\boldsymbol{\theta}^{11})\right], \\ \tilde{P}_{2g}(\boldsymbol{\theta}) &= \left[\tilde{P}(\boldsymbol{\theta}^{00}), \tilde{P}(\boldsymbol{\theta}^{10}), \tilde{P}(\boldsymbol{\theta}^{01}), \tilde{P}(\boldsymbol{\theta}^{11})\right]^T, \\ \tilde{S}_{2g}(\boldsymbol{\theta}) &= \text{diag}\left\{\tilde{S}(\boldsymbol{\theta}^{00}), \tilde{S}(\boldsymbol{\theta}^{10}), \tilde{S}(\boldsymbol{\theta}^{01}), \tilde{S}(\boldsymbol{\theta}^{11})\right\}. \end{aligned}$$

Here, $\text{diag}\{A_1, A_2, A_3, A_4\}$ is the diagonal matrix with diagonal entries, A_1, A_2, A_3 , and A_4 , and \tilde{A}_C is the symbol of the coarse-grid operator.

Definition 2. The two-grid LFA convergence factor, $\hat{\rho}$, is defined as

$$\hat{\rho} = \sup_{\boldsymbol{\theta} \in T^{\text{low}}} \rho\left(\tilde{E}_{2g}(\boldsymbol{\theta})\right), \quad (9)$$

where $\rho(\tilde{E}_{2g}(\boldsymbol{\theta}))$ denotes the spectral radius of matrix $\tilde{E}_{2g}(\boldsymbol{\theta})$.

In this work, we will apply LFA to the monolithic multigrid algorithms described above, and optimize the two-grid convergence factor using a robust optimization framework recently developed for cases such as this with multiple parameters to be optimized⁴¹. While we do not compute $\hat{\rho}$ from (9) exactly, we use this to denote the values obtained from the optimization algorithm that, necessarily, samples the spectral radius of $\tilde{E}_{2g}(\boldsymbol{\theta})$ at only a finite number of points.

4.2 | Fourier representation for $\mathbb{Q}_2/\mathbb{Q}_1$ and \mathbb{Q}_1 iso $\mathbb{Q}_2/\mathbb{Q}_1$ discretizations

LFA for coupled systems discretized using mixed finite-element approaches is necessarily more complicated than in the scalar case. While the staggered finite-difference case can be successfully handled using slight generalizations of the scalar case^{7, 30, 32}, greater adaptation is required for higher-order or otherwise non-nodal finite-element discretizations^{33, 34, 40, 42}. The key step is in realizing that the resulting discrete operators (including the infinite-grid analog of (3)) can be reordered into block structured linear systems with Toeplitz blocks. Once suitably reordered, each block can be diagonalized using the classical Fourier approach. In this way, LFA of more complicated operators in a two-grid method results in block Fourier symbols that can be assembled as in (8) and maximized to yield a two-grid LFA convergence factor, as in (9).

For the $\mathbb{Q}_2/\mathbb{Q}_1$ and $\mathbb{Q}_1\text{iso}\mathbb{Q}_2/\mathbb{Q}_1$ systems considered here, the natural structure is as 9×9 block systems. Consider the velocity DoFs as pictured in either Figure 1 or Figure 3; both the \mathbb{Q}_2 and $\mathbb{Q}_1\text{iso}\mathbb{Q}_2$ spaces have basis functions associated with the nodes of the quadrilateral mesh, as well as along horizontal and vertical mesh edges, and at the center of the mesh cells. Since there are 2 components (horizontal and vertical) to the velocity, this gives eight *types* of DoFs associated with the velocity discretization. The \mathbb{Q}_1 pressure gives the ninth set of DoFs in the block 9×9 structure. A key realization necessary for the LFA is that, when the system matrices (or their infinite-grid analogs) are reordered blockwise, each block in the reordered system has Toeplitz structure. Thus, we can diagonalize each block in the system by a Fourier transform, as discussed in Section 4.1. After diagonalizing the blocks, the system can be reordered frequency-wise, into a block operator with 9×9 blocks, by collecting all rows/columns corresponding to each Fourier frequency into adjacent rows/columns of the operator. If we further order the frequencies in harmonic sets, we get a block 36×36 structure associated with each harmonic space, $F(\theta)$. While analysis of the relaxation operators is most natural using the 9×9 block structure, complete analysis of the two-grid convergence factor requires use of the 36×36 block structure.

The block symbol for the $\mathbb{Q}_2/\mathbb{Q}_1$ Stokes discretization was derived in earlier work³⁴, as are symbols for the \mathbb{Q}_2 Laplacian and the canonical finite-element interpolation and restriction operators for the \mathbb{Q}_2 finite-element space⁴⁰. Symbols for both Braess-Sarazin³⁴ and additive Vanka¹⁷ relaxation for this discretization were also computed in earlier work. There is, in principle, very little different to computing these symbols for the $\mathbb{Q}_1\text{iso}\mathbb{Q}_2/\mathbb{Q}_1$ discretization. The reordered block structure of the $\mathbb{Q}_1\text{iso}\mathbb{Q}_2/\mathbb{Q}_1$ saddle point matrix is the same as that of the $\mathbb{Q}_2/\mathbb{Q}_1$ matrix. Once again, each individual block of the 9×9 system is a Toeplitz matrix, though the specific entries are now different than for the $\mathbb{Q}_2/\mathbb{Q}_1$ case. For example, a block row associated with one *type* of velocity DoF would have five nonzero blocks. If this *type* corresponds to horizontal velocity DoFs located at pressure cell centers (denoted by a diamond marker in Figure 1), then four of these nonzero blocks correspond to *types* associated with horizontal velocity DoFs and the fifth block corresponds to the gradient operator acting on the pressure. The diagonal block within this block row is itself diagonal, reflecting the fact that there are no matrix connections between different velocity *types* in the $\mathbb{Q}_1\text{iso}\mathbb{Q}_2$ Laplacian matrix. Referring to the right side of Figure 1, this corresponds to the fact that two adjacent velocity DoFs in the velocity mesh always have different markers. Two of the other nonzero velocity blocks within this same block row are Toeplitz matrices with only 2 nonzeros per row. Again referring to the right side of Figure 1, the nonzeros in one of these blocks correspond to stencil entries associated with the North and South horizontal velocity DoFs, located on the horizontal edges of the mesh, which share the same marker. The two nonzeros in the other block correspond to stencil entries associated with the East and West horizontal velocity DoFs, now on vertical edges of the mesh, which again share the same marker. The final nonzero velocity block in this same block row would have four nonzeros that correspond to stencil entries associated with the corner horizontal velocity DoFs, located at the nodes of the mesh, which all share the same marker. The Toeplitz block for the gradient operator mapping onto these velocity DoFs would have four nonzero entries per row, associated with the four nodal pressure DoFs for the cell. It should be noted that the number of nonzeros per row in a gradient Toeplitz block depends on the specific block row that is being considered, i.e. the particular velocity marker associated with the block row in Figure 1. For the stencil representation of each Toeplitz matrix, standard Fourier techniques, as described above, give the block-structured symbol of the operator. Similarly, the symbols for interpolation and restriction can be computed⁴⁰ in the $\mathbb{Q}_1\text{iso}\mathbb{Q}_2$ setting, and those for Braess-Sarazin³⁴ and additive Vanka¹⁷ relaxation as well. Since the full calculations are rather tedious, we omit the details, noting that there are existing software packages^{43, 44} that could be used to compute the symbols automatically.

5 | NUMERICAL RESULTS

To evaluate the effectiveness of $\mathbb{Q}_1\text{iso}\mathbb{Q}_2/\mathbb{Q}_1$ multigrid preconditioners for the $\mathbb{Q}_2/\mathbb{Q}_1$ system, we start by comparing LFA predicted two-grid convergence factors against measured convergence factors for the Stokes system with Dirichlet boundary conditions on a uniform square mesh with $h = \frac{1}{64}$. For convenience, the $\mathbb{Q}_2/\mathbb{Q}_1$ discretization matrices are assembled using Firedrake^{45, 46}, while the $\mathbb{Q}_1\text{iso}\mathbb{Q}_2/\mathbb{Q}_1$ discretization matrices are assembled by forming a finer-mesh $\mathbb{Q}_2/\mathbb{Q}_1$ discretization, then applying coarsening-in-order to the velocity DoFs and coarsening-in-space to the pressure DoFs. The defect-correction preconditioner is implemented as a GMG variant taken from the PyAMG library⁴⁷, with our own implementation of the relaxation schemes. The measured convergence factors are then computed by running the solver 100 times using a zero right-hand side and a different random initial guess each time. The vector ℓ^2 norm of the last $\min(m_s, 10)$ residuals are collected for each of the 100 runs, where m_s is the number of iterations required to reduce the residual by a factor of 10^{-10} for the s^{th} solve. When this criteria is not met in 100 iterations, we take $m_s = 100$. Collected residual norms are then fit by a linear least-squares model of

the form $\xi_0 + \xi_1 j = \ln r_{j_s}$ where r_{j_s} is the j^{th} residual within the $\min(m_s, 10)$ collected residuals from the s^{th} run. The averaged asymptotic convergence factor is then taken as $\rho = e^{\xi_1}$.

Within the multigrid cycle, the number of pre- and post-relaxation sweeps is always 1 for $\ell \geq 1$. To distinguish between different preconditioners based on (5), we focus on the triple (v_1, v_2, γ) , where v_1 and v_2 are the number of pre-/post- relaxation sweeps on the K_0 system, and γ is the number of h -multigrid cycles on the K_1 system. For fixed values of these parameters, we use the LFA optimization framework of Brown et al.⁴¹ to choose the remaining parameters in the method. Referring to (5), these parameters include a damping parameter for the $\mathbb{Q}_1 \text{ iso } \mathbb{Q}_2 / \mathbb{Q}_1$ cycling, τ , outer relaxation damping parameters for both the $\mathbb{Q}_2 / \mathbb{Q}_1$ and $\mathbb{Q}_1 \text{ iso } \mathbb{Q}_2 / \mathbb{Q}_1$ relaxation schemes and, if IBSR relaxation is used, inner relaxation parameters for that relaxation. The notation for these parameters is summarized in Table 1.

Symbol	Description
K_0	saddle point system for $\mathbb{Q}_2 / \mathbb{Q}_1$
K_1	saddle point system for $\mathbb{Q}_1 \text{ iso } \mathbb{Q}_2 / \mathbb{Q}_1$
K_ℓ	coarse saddle point $\mathbb{Q}_1 \text{ iso } \mathbb{Q}_2 / \mathbb{Q}_1$ system for $\ell \geq 2$
M_ℓ	relaxation operator on level ℓ
v_1	number of pre-relaxation sweeps used on the K_0 system
v_2	number of post-relaxation sweeps used on the K_0 system
γ	number of h -multigrid cycles used to solve the K_1 system
τ	$\mathbb{Q}_1 \text{ iso } \mathbb{Q}_2 / \mathbb{Q}_1$ -cycle solution damping parameter on level 1
α_0	Inexact Braess-Sarazin (IBS) relaxation parameter on level 0
β_0	weighted Jacobi relaxation parameter in IBSR on level 0
ω_0	relaxation global update parameter on level 0
α_1	Braess-Sarazin (BS) relaxation parameter for all $\ell \geq 1$
β_1	BS weighted Jacobi relaxation parameter for all $\ell \geq 1$
ω_1	relaxation global update parameter for all $\ell \geq 1$
$\hat{\rho}$	LFA predicted two-grid convergence factor
ρ	measured convergence factor for Dirichlet BC problem
m	measured iteration count for multigrid or preconditioned FGMRES
superscript P	problem with periodic boundary conditions

TABLE 1 Notation Reference Table

5.1 | Two-grid Results

We start by verifying that the measured two-grid convergence factors, ρ , agree with the LFA predictions, $\hat{\rho}$. Table 2 demonstrates that there is generally good agreement. As expected, we also see that increasing the number of K_0 relaxation sweeps improves convergence. For example, increasing the number of IBSR sweeps from $(v_1, v_2, \gamma) = (1, 0, 1)$ to $(v_1, v_2, \gamma) = (2, 2, 1)$ improves the measured convergence factor from 0.16 to 0.05. Similar V-cycles for Vanka relaxation demonstrate an analogous trend, where the convergence factor decreases from 0.31 to 0.15. Interestingly, there is some notable variation in both the damping parameter, τ , and the outer relaxation weights ω_ℓ . In results not reported here, the optimal value for τ was found to be 1/2 for a simpler preconditioner with error-propagation operator $I - \tau K_1^{-1} K_0$ (i.e., taking $v_1 = v_2 = 0$ and $\gamma \rightarrow \infty$). Here, we see that adding relaxation on the K_0 system and using a more practical approximation to K_1^{-1} result in values for τ much closer to 1. Depending on the (v_1, v_2, γ) values, we see values for ω_ℓ varying in the range from roughly 1/2 to 1, and similar variations in the inner IBSR parameters.

In order to test whether relaxation on both the K_0 and K_1 systems is necessary for robust convergence, we eliminate the relaxation on one of these systems by setting either $\omega_0 = 0$ or $\omega_1 = 0$. The results in Table 3 suggest that removing the K_0

TABLE 2 LFA predictions ($\hat{\rho}$) compared with the measured convergence factors (ρ) for inexact Braess-Sarazin (BS) and Vanka (V) relaxation. As α_ℓ and β_ℓ are only needed for IBSR relaxation, we do not record values of these parameters for Vanka relaxation.

	ν_1	ν_2	γ	τ	ω_0	ω_1	α_0	β_0	α_1	β_1	$\hat{\rho}$	ρ
BS	1	0	1	.87	1.02	.90	1.20	.79	.74	.88	.18	.16
	1	0	2	.86	.75	1.04	.99	.70	1.15	.88	.20	.18
	1	1	1	.97	.91	1.04	1.02	.93	.78	.86	.09	.11
	2	2	1	1.04	.55	.59	.72	.99	.85	1.30	.04	.05
V	1	0	1	.86	.78	1.01	-	-	-	-	.37	.31
	1	0	2	.90	.98	.83	-	-	-	-	.21	.20
	1	0	3	.85	1.02	.82	-	-	-	-	.20	.19
	1	1	1	.99	.67	.93	-	-	-	-	.29	.27
	1	1	2	1.05	.74	.78	-	-	-	-	.12	.09
	2	2	1	0.98	.71	1.05	-	-	-	-	.16	.15

relaxation is more detrimental to convergence than removing relaxation on the K_1 system. Specifically, we compare $(\nu_1, \nu_2, \gamma) = (0, 0, 1)$ and $\omega_0 = 0$ with $(\nu_1, \nu_2, \gamma) = (1, 1, 1)$ and $\omega_1 = 0$. In this case, there is a single pre- and post-relaxation in the cycle, on either the $\mathbb{Q}_1 \text{ iso } \mathbb{Q}_2 / \mathbb{Q}_1$ or $\mathbb{Q}_2 / \mathbb{Q}_1$ system. Similarly, we compare $(\nu_1, \nu_2, \gamma) = (0, 0, 2)$ and $\omega_0 = 0$ with $(\nu_1, \nu_2, \gamma) = (2, 2, 1)$ and $\omega_1 = 0$. Here, there are now two pre- and post-relaxation sweeps in the cycle on either the $\mathbb{Q}_1 \text{ iso } \mathbb{Q}_2 / \mathbb{Q}_1$ or $\mathbb{Q}_2 / \mathbb{Q}_1$ system, although using $\gamma = 2$ results in one additional coarse-grid correction in comparison to the $\gamma = 1$ case. We emphasize that setting $\omega_1 = 0$ omits only relaxation on the “fine grid” K_1 system in the two-level method. In the case of Braess-Sarazin with $\omega_0 = 0$ and $\gamma = 2$, the predicted convergence factor is 0.52 compared with 0.11 for relaxation only on K_0 using $(\nu_1, \nu_2, \gamma) = (2, 2, 1)$. Similar V-cycles for Vanka relaxation demonstrate less of a convergence factor reduction from 0.57 to 0.29. We also note that some of the measured convergence factors deviate from the LFA predictions in the case of Braess-Sarazin, while measured Vanka results agree closely with the LFA predictions. The two-grid convergence factors for periodic boundary condition problems are expected to match the predicted values exactly^{30, 48, 49}, while sometimes a gap between the LFA predicted factors and the measured factors is observed for the Dirichlet boundary condition case^{30, 34}.

TABLE 3 Effect of omitting relaxation on K_0 and K_1 . $\omega_0 = 0$ corresponds only relaxation on the $\mathbb{Q}_1 \text{ iso } \mathbb{Q}_2 / \mathbb{Q}_1$ system, while $\omega_1 = 0$ corresponds to only relaxation on the $\mathbb{Q}_2 / \mathbb{Q}_1$ system.

	ν_1	ν_2	γ	τ	ω_0	ω_1	α_0	β_0	α_1	β_1	$\hat{\rho}$	ρ
BS	0	0	1	.93	0	.24	-	-	.67	1.56	.60	.65
	0	0	2	.63	0	.40	-	-	.52	1.35	.52	.51
	1	1	1	.77	.45	0	.46	1.37	-	-	.32	.52
	2	2	1	.99	.85	0	.90	1.12	-	-	.11	.41
V	0	0	1	.64	0	.98	-	-	-	-	.63	.65
	0	0	2	.66	0	.63	-	-	-	-	.57	.55
	1	1	1	.48	.81	0	-	-	-	-	.56	.51
	2	2	1	.80	.85	0	-	-	-	-	.29	.25

Considering the information in Tables 2 and 3, we compare whether relaxation on both K_0 and K_1 is necessary or relaxation on K_0 system is sufficient. For example, Vanka relaxation with $(\nu_1, \nu_2, \gamma) = (1, 1, 1)$ in Table 2 relaxes on both systems, while taking $(\nu_1, \nu_2, \gamma) = (2, 2, 1)$ with $\omega_1 = 0$ in Table 3 use the same total number of relaxation sweeps, but only on the K_0 system. Their convergence factors are comparable, giving 0.27 and 0.25, respectively. For Braess-Sarazin, the LFA predicted

performance for the same cycle types is also comparable, giving 0.09 and 0.11 , respectively. However, the measured Braess-Sarazin convergence factors deviate quite significantly from these predictions. Since there appears to be little benefit to omitting this relaxation even in the ideal setting of periodic boundary conditions, and potentially significant degradation in performance when used with Dirichlet boundary conditions, we do not consider the methods from Table 3 further and, instead, focus on methods where we allow relaxation on both K_0 and K_1 .

Remark 1. Comparison with direct application of GMG to the $\mathbb{Q}_2/\mathbb{Q}_1$ discretization. The hp -multigrid convergence rates that we report are quite similar to the $\mathbb{Q}_2/\mathbb{Q}_1$ h -multigrid results reported in earlier work^{34,50}. For Vanka relaxation, our two-grid cycle $(1, 1, 1)$ has the same total number of fine-level relaxation sweeps (considering both K_0 and K_1) as a $(2, 2)$ h -multigrid cycle, where a total of two pre- and two post-relaxation sweeps are performed. The measured convergence factor for a unit square domain with periodic boundary conditions is reported as 0.29 for the h -multigrid solver⁵⁰, which exactly matches our results. For IBSR based GMG, a measured convergence factor of 0.09 is reported³⁴ with an h -multigrid $(2, 2)$ cycle for a problem on a unit square domain with Dirichlet boundary conditions, which closely matches our rate of $.11$ for a $(1, 1, 1)$ cycle in Table 3. Here, small differences could potentially arise due to the different number of weighted-Jacobi sweeps in the computation of the pressure correction (two sweeps for the h -multigrid benchmark versus one for our method). Overall, however it is clear that comparable convergence rates are obtained when either GMG is applied directly to the $\mathbb{Q}_2/\mathbb{Q}_1$ discretization or when it is applied indirectly via an intermediate \mathbb{Q}_1 iso $\mathbb{Q}_2/\mathbb{Q}_1$ system.

In order to study the convergence rate sensitivity to parameter choices, we consider the two-grid convergence factor for the same Dirichlet boundary value problem as in the previous section. In case of Vanka relaxation, we consider the $V(1, 1, 2)$ cycle from Table 2, where we fix τ and vary ω_0 and ω_1 from 0.02 to 1.0 . In the left plot of Figure 4, we observe poor performance for the majority of ω_1 values when ω_0 is “too small”. However, for larger values of ω_0 , the performance becomes less sensitivity to perturbation in ω_1 . Multigrid solvers using inexact Braess-Sarazin relaxation have many more parameters than Vanka, which makes the sensitivity analysis slightly more complicated. For simplicity, we fix τ , α_i , and β_i to be the same as in cycle $BS(2, 2, 1)$ in Table 2, while varying ω_0 and ω_1 . As seen in the right plot of Figure 4, there is a large region where we see near-optimal $BS(2, 2, 1)$ convergence without having to re-optimize the α_i and β_i . This suggests that the performance of $BS(2, 2, 1)$ is not too sensitive to its parameters. We note that, for both relaxation schemes, there is a clear advantage to an informed choice of the relaxation parameters over naive choices, such as $\omega_0 = \omega_1 = 1$, but the sensitivity to their choices is not so severe as to be a practical drawback to using these approaches.

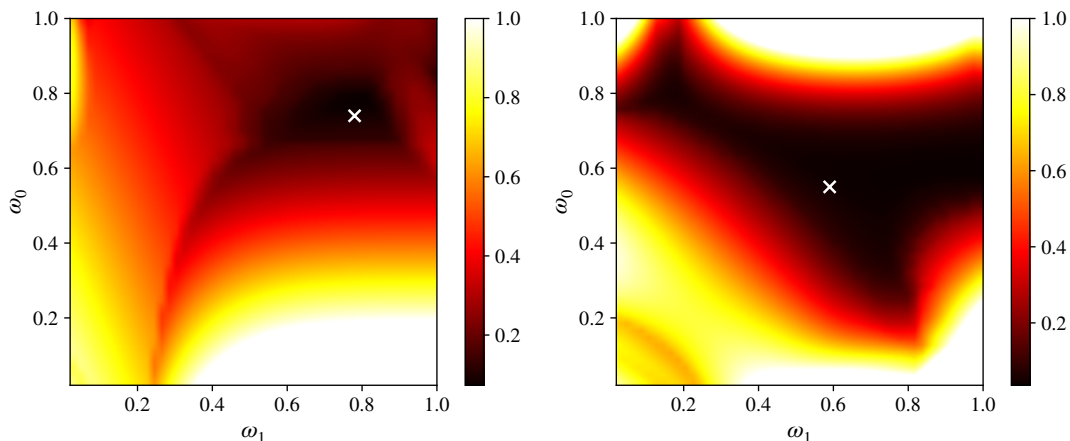


FIGURE 4 Sensitivity analysis of the measured two-grid convergence factors for $V(1, 1, 2)$ (left) and $BS(2, 2, 1)$ (right) cycles.

5.2 | Multilevel results

We now consider five-level algorithms, where the coarsest grid is a 4×4 mesh. The test problem is the same as in the previous subsection, with a uniform grid on the unit square and $h = \frac{1}{64}$. We use the same parameters from Table 2 and compare the

multilevel convergence results against both the LFA predicted two-grid convergence factors and the two-level performance reported above. The multilevel algorithm is formed by recursively extending the h -multigrid hierarchy in operator G_1 . For completeness, Table 4 measures both V- and W-cycle convergence factors for stationary multigrid iterations, as well as the number of iterations required to reduce the norm of the absolute residual based on K_0 to 10^{-10} , using both stationary GMG iterations and multigrid preconditioned FGMRES. The measured convergence factors for W-cycles presented in Table 4 agree with the LFA predicted results above. The V-cycle convergence rates, on the other hand, tend to underperform for both periodic and Dirichlet boundary conditions. Even though the W-cycle preconditioned FGMRES solver tends to converge in the fewest number of iterations, the difference in iteration counts is not large, suggesting that V-cycle preconditioned FGMRES may be the more computationally efficient approach³⁰, particularly in a parallel setting. We note that the large discrepancy between the number of iterations required for convergence using stationary V-cycles and V-cycle preconditioned FGMRES suggests that there are only a few modes that are not well-captured by the GMG operators.

TABLE 4 Predicted two-grid LFA convergence factors and measured convergence estimates for the multilevel method applied to the unit-square test problem. A P superscript denotes use of periodic boundary conditions, while no superscript denotes Dirichlet boundary conditions. The last four columns list iteration counts to achieve a relative residual reduction tolerance using either stationary GMG iterations or GMG as a preconditioner for FGMRES.

							GMG		w/ FGMRES	
ν_1	ν_2	γ	Cycle	$\hat{\rho}$	ρ^P	ρ	m^P	m	m^P	m
BS	1	0	V	.18	.17	.20	13	14	12	12
			W				13	13	12	12
	1	1	V	.09	.25	.55	13	33	9	11
			W				9	10	8	9
V	1	0	V	.21	.47	.20	21	14	12	11
			W				14	14	11	11
	1	1	V	.12	.18	.18	12	12	10	10
			W				10	10	9	9

We note that these results use damping parameters obtained from the two-level analysis. As the two-level analysis assumes exact coarse-grid solves and W-cycles are expected to provide more accurate coarse solution than V-cycles, the W-cycle case is somewhat closer to the assumptions underlying the two-level analysis. From this viewpoint, the better performance of the W-cycles is not surprising. Given the observed success using V-cycles as preconditioners for FGMRES, we have not undertaken a multilevel LFA to see if there might possibly be better parameter choices for the V-cycle.

5.3 | Stokes backward-facing step problem

In this section, we consider the performance of the preconditioned FGMRES algorithms as we increase the fine-scale problem size and number of levels in the multigrid hierarchy. For this test, we consider a backward-facing step domain with the solution strategies discussed in Section 5.2 and verify that the resulting iteration counts are relatively stable with respect to mesh refinement. For all tests, the Stokes problem is defined on a backward-facing step domain with a parabolic inflow and natural outflow boundary conditions. A Poiseuille flow profile is imposed on the inflow boundary ($x = 0; 0 \leq y \leq 2$). A homogeneous Neumann boundary condition is imposed on the outflow boundary ($x = 2; 0 \leq y \leq 2$), thereby fixing the mean outflow pressure to be zero. No-slip (zero velocity) boundary conditions are imposed on all other boundary faces. More details on this type of problem can be found, for example, in Elman et al.¹.

Table 5 summarizes the results, presenting iteration counts for multigrid preconditioned FGMRES. Using both IBSR and Vanka as relaxation within the preconditioner, we perform V- and W-cycle convergence tests with respect to problem size. The relaxation parameters are picked based on the most successful multilevel convergence results in Section 5.2. The parameter values for these two multigrid hierarchies can be found in Tables 2 and 3 under the corresponding (ν_1, ν_2, γ) values: (1, 1, 1)

for Braess-Sarazin and $(1, 1, 2)$ for Vanka relaxation. For both IBSR and Vanka relaxation, the V-cycle results exhibit modest iteration growth as the problem size is increased. The convergence results for the W-cycle tests show constant iteration counts.

TABLE 5 FGMRES iterations to convergence for backward-facing step problem. Braess-Sarazin relaxation parameters are based on the results in Table 2. Vanka relaxation parameters are based on the results in Table 4.

DoFs	GMG levels	Method, (v_1, v_2, γ)			
		BS, $(1, 1, 1)$		V, $(1, 1, 2)$	
		V-cycle	W-cycle	V-cycle	W-cycle
515	2	10	10	9	10
1891	3	11	10	10	10
7235	4	12	10	11	10
28 291	5	13	10	11	10
111 875	6	14	10	12	10
444 931	7	16	10	14	10

In addition to the number of FGMRES iterations in Table 5, we present the solve phase timings for Vanka and Braess-Sarazin based solvers in Figure 5. Both solvers's timings scale proportionally with the number of DoFs in the system and the total number of FGMRES iterations. While a single W-cycle is more computationally expensive per iteration than a V-cycle, the degradation in performance when using V-cycles makes W-cycles the faster option, due to the constant number of iterations to convergence. This is true for both Braess-Sarazin and Vanka based multigrid cycles. While we see generally faster times for the Braess-Sarazin cycles here, we refrain from drawing conclusions about the relative performance between the two relaxation schemes, because timings are highly dependent on the specifics of their implementation and optimization³⁹.

6 | CONCLUSIONS AND FUTURE WORK

In this paper, we demonstrate that the low-order, \mathbb{Q}_1 iso $\mathbb{Q}_2/\mathbb{Q}_1$, finite-element discretization can be used to construct effective preconditioners for the higher-order $\mathbb{Q}_2/\mathbb{Q}_1$ finite-element discretization of the Stokes equations. To achieve effective performance, we use LFA in combination with robust optimization algorithms to compute relaxation parameters that optimize the resulting two-grid convergence factors for various two-grid algorithms based on the \mathbb{Q}_1 iso $\mathbb{Q}_2/\mathbb{Q}_1$ hierarchy of grids. The measured two-grid convergence factors for both periodic and Dirichlet boundary conditions generally agree quite closely with the LFA-predicted two-grid convergence factors. For multilevel convergence, we observe close agreement between the measured W-cycle convergence factors and the LFA predictions. The V-cycle multilevel convergence factors, however, can deviate significantly more from the LFA predictions than the W-cycle. Both V- and W-cycles, however, lead to effective preconditioners for FGMRES for some parameter choices. When used on a more challenging backward-facing step problem, W-cycle preconditioned FGMRES leads to no growth in iteration counts as the mesh is refined, while modest growth in iterations is seen with V-cycle preconditioners. Hence for the large problem sizes, W-cycle preconditioned FGMRES solvers are faster.

An immediate next step in this research is to see whether these results can be leveraged in the development of monolithic AMG algorithms for the $\mathbb{Q}_2/\mathbb{Q}_1$ discretization of the Stokes equations. Despite a long history of research effort, there has been little success in developing true algebraic MG approaches for saddle-point systems such as these. Preliminary numerical results, that we intend to report in a future manuscript, suggest that it is easier to develop AMG algorithms for the \mathbb{Q}_1 iso $\mathbb{Q}_2/\mathbb{Q}_1$ discretization as we consider here. If successful, further work is possible for higher-order discretizations, such as the Scott-Vogelius discretization of the (Navier-) Stokes equations^{51, 52}, or for coupled systems of equations of saddle-point type, such as viscoresistive magnetohydrodynamics⁵³.

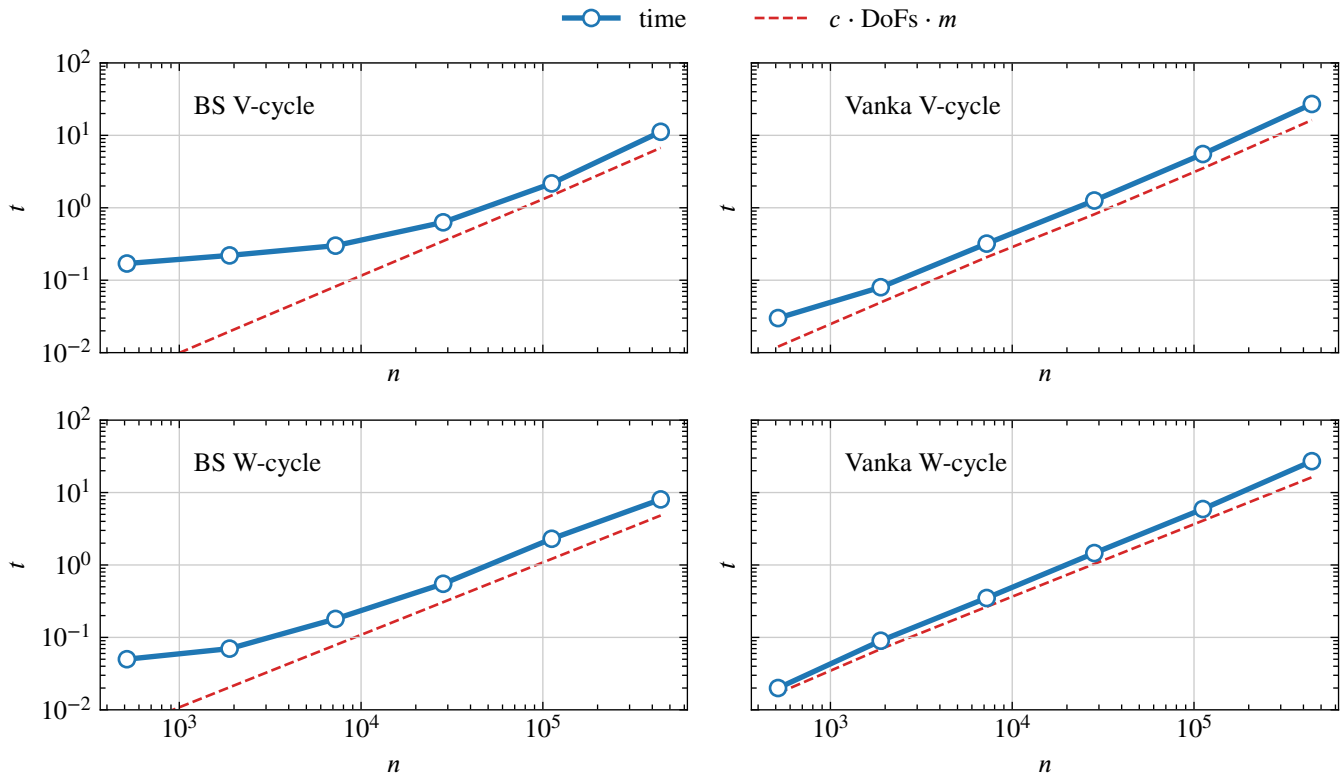


FIGURE 5 Timing of Braess-Sarazin and Vanka relaxation-based V- and W-cycles. The dashed line represents the scaling with problem size in the form of $c \cdot \text{DoFs} \cdot m$, for some constant c and where m is the number of FGMRES iterations.

The source code used to collect data for this paper is publicly available at https://github.com/lexeyV/Stokes_isoQ2Q1. It is implemented in Python 3 under the 3-Clause BSD License. Version 1.0 is used in this paper, under commit 6ba1fa393dcdca113a011453630695afa49c9dfd.

ACKNOWLEDGMENTS

The work of SPM was partially supported by an NSERC Discovery Grant. RT was supported by the U.S. Department of Energy, Office of Science, Office of Advanced Scientific Computing Research, Applied Mathematics program. Sandia National Laboratories is a multimission laboratory managed and operated by National Technology and Engineering Solutions of Sandia, LLC., a wholly owned subsidiary of Honeywell International, Inc., for the U.S. Department of Energy's National Nuclear Security Administration under grant DE-NA-0003525. This paper describes objective technical results and analysis. Any subjective views or opinions that might be expressed in the paper do not necessarily represent the views of the U.S. Department of Energy or the United States Government.

References

1. Elman HC, Silvester DJ, and Wathen AJ. Finite elements and fast iterative solvers: with applications in incompressible fluid dynamics. Oxford University Press, USA; 2014.
2. Benzi M, Golub GH, and Liesen J. Numerical solution of saddle point problems. *Acta Numer.* 2005;**14**:1–137.
3. Brandt A, and Dinar N. Multigrid solutions to elliptic flow problems. In: Parter S, editor. *Numerical Methods for Partial Differential Equations*. New York: Academic Press; 1979. p. 53–147.

4. Brandt A. Multigrid techniques: 1984 guide with applications to fluid dynamics. GMD–Studien Nr. 85. St. Augustin: Gesellschaft für Mathematik und Datenverarbeitung; 1984.
5. Vanka SP. Block-implicit multigrid solution of Navier-Stokes equations in primitive variables. *J Comput Phys.* 1986;**65**:138–158.
6. Linden J, Lonsdale G, Steckel B, and Stüben K. Multigrid for the steady-state incompressible Navier-Stokes equations: a survey. In: 11th International Conference on Numerical Methods in Fluid Dynamics (Williamsburg, VA, 1988). vol. 323 of Lecture Notes in Phys. Berlin: Springer; 1989. p. 57–68.
7. Niestegge A, and Witsch K. Analysis of a multigrid Stokes solver. *Appl Math Comput.* 1990;**35**(3):291–303.
8. Braess D, and Sarazin R. An efficient smoother for the Stokes problem. *Applied Numerical Mathematics.* 1997;**23**(1):3–19.
9. John V, and Tobiska L. Numerical performance of smoothers in coupled multigrid methods for the parallel solution of the incompressible Navier-Stokes equations. *International Journal For Numerical Methods In Fluids.* 2000 Jan;**33**(4):453–473.
10. Wabro M. Coupled algebraic multigrid methods for the Oseen problem. *Comput Vis Sci.* 2004;**7**(3-4):141–151.
11. Wabro M. AMGc—coarsening strategies and application to the Oseen equations. *SIAM J Sci Comput.* 2006;**27**(6):2077–2097.
12. Larin M, and Reusken A. A comparative study of efficient iterative solvers for generalized Stokes equations. *Numer Linear Algebra Appl.* 2008;**15**(1):13–34.
13. Janka A. Smoothed aggregation multigrid for a Stokes problem. *Comput Vis Sci.* 2008;**11**(3):169–180.
14. Gmeiner B, Huber M, John L, Rüde U, and Wohlmuth B. A quantitative performance study for Stokes solvers at the extreme scale. *J Comput Sci.* 2016;**17**(part 3):509–521. Available from: <https://doi.org/10.1016/j.jocs.2016.06.006>.
15. Adler JH, Benson TR, and MacLachlan SP. Preconditioning a mass-conserving discontinuous Galerkin discretization of the Stokes equations. *Numerical Linear Algebra with Applications.* 2017;**24**(3):e2047.
16. Prokopenko A, and Tuminaro RS. An algebraic multigrid method for Q_2 - Q_1 mixed discretizations of the Navier-Stokes equations. *Numerical Linear Algebra with Applications.* 2017;**24**(6):e2109.
17. Farrell PE, He Y, and MacLachlan S. A local Fourier analysis of additive Vanka relaxation for the Stokes equations. *Numer Linear Alg Appl.* 2020; To appear, <https://doi.org/10.1002/nla.2306>.
18. Epperly EN, Barker AT, and Falgout RD. 2020. *Smoothers for Matrix-Free Algebraic Multigrid Preconditioning of High-Order Finite Elements*. LLNL-TR-814531. Lawrence Livermore National Laboratory.
19. Heys J, Manteuffel T, McCormick SF, and Olson L. Algebraic multigrid for higher-order finite elements. *Journal of computational Physics.* 2005;**204**(2):520–532.
20. Deville MO, and Mund EH. Finite-element preconditioning for pseudospectral solutions of elliptic problems. *SIAM Journal on Scientific and Statistical Computing.* 1990;**11**(2):311–342.
21. Napov A, and Notay Y. Algebraic multigrid for moderate order finite elements. *SIAM Journal on Scientific Computing.* 2014;**36**(4):A1678–A1707.
22. Olson L. Algebraic multigrid preconditioning of high-order spectral elements for elliptic problems on a simplicial mesh. *SIAM Journal on Scientific Computing.* 2007;**29**(5):2189–2209.
23. Orszag SA. Spectral methods for problems in complex geometrics. In: Numerical methods for partial differential equations. Elsevier; 1979. p. 273–305.
24. Xu J. The auxiliary space method and optimal multigrid preconditioning techniques for unstructured grids. *Computing.* 1996;**56**(3):215–235.

25. John V, Knobloch P, Matthies G, and Tobiska L. Non-nested multi-level solvers for finite element discretisations of mixed problems. *Computing*. 2002;**68**(4):313–341.
26. Hackbusch W. On multi-grid iterations with defect correction. In: Hackbusch W, and Trottenberg U, editors. *Multigrid Methods*. Berlin, Heidelberg: Springer Berlin Heidelberg; 1982. p. 461–473.
27. Koren B. Multigrid and defect correction for the steady Navier-Stokes equations. *Journal of Computational Physics*. 1990;**87**(1):25–46. Available from: <https://www.sciencedirect.com/science/article/pii/002199919090223N>.
28. Benzi M, and Olshanskii MA. An augmented Lagrangian-based approach to the Oseen problem. *SIAM Journal on Scientific Computing*. 2006;**28**(6):2095–2113.
29. Emami M. Efficient Multigrid Solvers for the Stokes Equations using FiniteElements. *Lehrstuhl für Informatik 10 (Systemsimulation)*. 2013;.
30. Trottenberg U, Oosterlee CW, and Schüller A. *Multigrid*. Academic Press, Inc., San Diego, CA; 2001.
31. Wienands R, and Joppich W. *Practical Fourier analysis for multigrid methods*. CRC press; 2004.
32. Sivaloganathan S. The use of local mode analysis in the design and comparison of multigrid methods. *Comput Phys Commun*. 1991;**65**:246–252.
33. MacLachlan SP, and Oosterlee CW. Local Fourier analysis for multigrid with overlapping smoothers applied to systems of PDEs. *Numer Linear Alg Appl*. 2011;**18**:751–774.
34. He Y, and MacLachlan SP. Local Fourier analysis for mixed finite-element methods for the Stokes equations. *Journal of Computational and Applied Mathematics*. 2019;**357**:161–183.
35. Ern A, and Guermond JL. *Theory and Practice of Finite Elements*. vol. 159 of *Applied Mathematical Sciences*. Springer-Verlag New York; 2004.
36. Deville MO, Fischer PF, Mund E, et al. *High-order methods for incompressible fluid flow*. vol. 9. Cambridge university press; 2002.
37. Deville MO, and Mund EH. Fourier analysis of finite element preconditioned collocation schemes. *SIAM journal on scientific and statistical computing*. 1992;**13**(2):596–610.
38. Farrell PE, Knepley MG, Mitchell L, and Wechsung F. PCPATCH: software for the topological construction of multigrid relaxation methods. *arXiv preprint arXiv:191208516*. 2019;.
39. Farrell PE, Knepley MG, Mitchell L, and Wechsung F. PCPATCH: software for the topological construction of multigrid relaxation methods. *arXiv preprint arXiv:191208516*. 2019;.
40. He Y, and MacLachlan SP. Two-level Fourier analysis of multigrid for higher-order finite-element discretizations of the Laplacian. *Numerical Linear Algebra with Applications*. 2020;**27**(3). E2285.
41. Brown J, He Y, MacLachlan SP, Menickelly M, and Wild S. Tuning multigrid methods with Robust optimization and local Fourier analysis. *SIAM Journal on Scientific Computing*. 2021;**43**(1):A109–A138.
42. Rodrigo C, Gaspar FJ, and Lisbona FJ. On a local Fourier analysis for overlapping block smoothers on triangular grids. *Appl Numer Math*. 2016;**105**:96–111.
43. Bolten M, and Rittich H. Fourier analysis of periodic stencils in multigrid methods. *SIAM J Sci Comput*. 2018;**40**(3):A1642–A1668.
44. Kahl K, and Kintscher N. Automated local Fourier analysis (aLFA). *BIT*. 2020;**60**(3):651–686.
45. Rathgeber F, Ham DA, Mitchell L, Lange M, Luporini F, Mcrae ATT, et al. Firedrake: Automating the Finite Element Method by Composing Abstractions. *ACM Trans Math Softw*. 2016 Dec;**43**(3):24:1–24:27. Available from: <http://doi.acm.org/10.1145/2998441>.

46. Kirby RC, and Mitchell L. Solver composition across the PDE/linear algebra barrier. *SIAM Journal on Scientific Computing*. 2018;**40**(1):C76–C98.
47. Olson LN, and Schroder JB. *PyAMG: Algebraic Multigrid Solvers in Python v4.0*; 2018. Release 4.0. Available from: <https://github.com/pyamg/pyamg>.
48. Stevenson RP. On the validity of local mode analysis of multi-grid methods (PhD dissertation). Utrecht University. Utrecht, The Netherlands; 1990.
49. Rodrigo C, Gaspar FJ, and Zikatanov LT. On the validity of the local Fourier analysis. *J Comput Math*. 2019;**37**(3):340–348.
50. Farrell PE, He Y, and MacLachlan SP. A local Fourier analysis of additive Vanka relaxation for the Stokes equations. *Numerical Linear Algebra with Applications*. 2020;p. e2306.
51. Scott, L R , and Vogelius, M . Norm estimates for a maximal right inverse of the divergence operator in spaces of piecewise polynomials. *ESAIM: M2AN*. 1985;**19**(1):111–143. Available from: <https://doi.org/10.1051/m2an/1985190101111>.
52. Farrell PE, Mitchell L, Scott LR, and Wechsung F. A Reynolds-robust preconditioner for the Scott-Vogelius discretization of the stationary incompressible Navier-Stokes equations. *The SMAI journal of computational mathematics*. 2021;**7**:75–96.
53. Adler JH, Benson T, Cyr EC, Farrell PE, MacLachlan S, and Tuminaro R. Monolithic Multigrid for Magnetohydrodynamics. *SIAM J Sci Comput*. 2021;To appear.
54. Voronin A, He Y, MacLachlan S, Olson LN, and Tuminaro R. Low-order preconditioning of the Stokes equations; 2021. https://github.com/lexeyV/Stokes_isoQ2Q1.